

Nova Experiments Examining Rayleigh-Taylor Instability in Materials with Strength

S.V. Weber, D.H. Kalantar, J.D. Colvin, D.M. Gold, K.O. Mikaelian, B.A. Remington, L.G. Wiley

This article was submitted to
7th International Workshop on the Physics of Compressible
Turbulent Mixing, Russian Federal Nuclear Center Institute of
Experimental Physics, St. Petersburg, Russia, July 5-9, 1999

U.S. Department of Energy

October 6, 1999

Lawrence
Livermore
National
Laboratory

DISCLAIMER

This document was prepared as an account of work sponsored by an agency of the United States Government. Neither the United States Government nor the University of California nor any of their employees, makes any warranty, express or implied, or assumes any legal liability or responsibility for the accuracy, completeness, or usefulness of any information, apparatus, product, or process disclosed, or represents that its use would not infringe privately owned rights. Reference herein to any specific commercial product, process, or service by trade name, trademark, manufacturer, or otherwise, does not necessarily constitute or imply its endorsement, recommendation, or favoring by the United States Government or the University of California. The views and opinions of authors expressed herein do not necessarily state or reflect those of the United States Government or the University of California, and shall not be used for advertising or product endorsement purposes.

Nova Experiments Examining Rayleigh-Taylor Instability in Materials with Strength

S. V. Weber, D. H. Kalantar, J. D. Colvin, D. M. Gold, K. O. Mikaelian, B. A. Remington, and L. G. Wiley,
Lawrence Livermore National Laboratory, Livermore, CA 94551-0808, USA
E-mail: svweber@llnl.gov

Abstract: Material strength can affect the growth of the Rayleigh-Taylor instability in solid materials^{1,2}, where growth occurs through plastic flow. In order to study this effect at megabar pressures, we have shocked metal foils using hohlraum x-ray drive on Nova, and observed the growth of pre-imposed modulations with x-ray radiography. Previous experiments employing Cu foils³ did not conclusively show strength effects for resolvable wavelengths. Therefore, we have redesigned the experiment to use aluminum foils. As aluminum has higher specific strength at pressures ~1 Mbar, the new design is predicted to show growth reduction due to strength of at least a factor of two for some wavelengths in the observable range of 10 - 50 μm . We have also modified the drive history to extend the interval of uniform acceleration and to reduce the risk of melting the foils with coalesced shocks. The design changes, as well as Nova operational constraints, limit peak pressures to 1-1.5 Mbar. Foil surface motion has been measured with high sensitivity by laser interferometry to look for thermal expansion due to preheat. We have continued to pursue dynamic x-ray diffraction as the most definitive measurement of crystal state.

1. Introduction

The Rayleigh-Taylor (RT) instability occurs when a light fluid accelerates a heavy fluid, and results in exponential growth of modulations at the interface between the two fluids. Material strength influences the growth of this instability in solids. If stresses do not exceed the yield strength of the material, the instability is stabilized, while if stresses are higher, growth will occur by plastic flow but at a lower rate than for a classical fluid. RT growth in strong materials has importance in geophysics, such as for cratering⁴ and for flows in the earth's interior⁵, in some engineering applications including explosive welding⁶, as well as having interest as fundamental materials dynamics.

Barnes et al.¹ examined stability of Al plates with machined surface perturbations which were accelerated by explosives. They observed the transition between stability and growth modified by strength. More extensive experiments of this type have been reported by Lebedev et al.² Nizovtsev and Rayevski⁷ present theoretical analysis of the stability boundary. Stability occurs for perturbation amplitudes less than the critical amplitude of $\eta_{th} = \eta_c(1 - 0.856e^{-kh/\sqrt{3}})[(1 - e^{-kh/\sqrt{3}})^2 - (\lambda/\lambda_c)^2]$ where $\lambda_c = 4\pi\mu/\rho g$, $\eta_c = 2Y/\rho g$, $k=2\pi/\lambda$ is the modulation wavenumber, h is the foil thickness, g is the acceleration, ρ is the density, μ is the shear modulus, and Y is the yield strength. Also, stability can only occur for $\lambda < \lambda_{th} = 2\lambda_c/[1 + 8\sqrt{3}c^2/gh]^{1/2}$, where c is the sound speed. Thus, the stability is dependent upon the constitutive model of the material as well as upon the parameters of the experiment.

A constitutive model, such as that of Steinberg⁸, describes dynamic material response, and specifies properties such as shear modulus and strength. Strength properties for materials may be measured by several methods. Quasistatic properties at high pressures may be measured on diamond anvils, while dynamic response has usually been measured by flier plates experiments using gas guns or explosives. Lasers offer a platform for reaching pressures and strain rates higher than those which have been achieved by other means. Such experiments could test material strength parameters in a new regime.

We have been conducting experiments on the Nova laser to examine RT instability in metal foils at pressures greater than 1 Mbar. Earlier experiments using Cu foils³ were presented at the Marseilles meeting. Effects of strength in those experiments were not large enough to be resolved. Therefore, we developed a new experiment design using Al foils and modified drive conditions. In this paper, we present details of the target design, x-ray drive characterization, and growth measurements for experiments using Cu and Al foils.

2. Experimental conditions

The geometry of the experiment is shown in Figure 1. The Nova experiments were conducted using x-ray drive in cylindrical gold hohlraums. Eight beams of the laser shone into the ends of the cylinder, producing x-rays with a nearly Planckian spectrum. A hydrodynamic package, consisting of an ablator of CH doped with 2% Br, pressed in

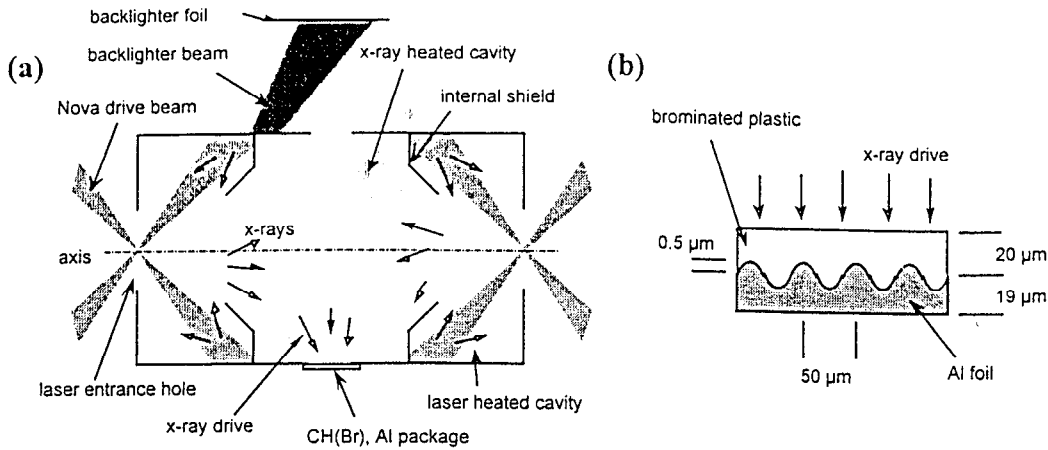


Figure 1. Experiment geometry (a) hohlraum target; (b) Rayleigh-Taylor package

contact with a metal foil, was mounted over a hole in the central wall of the cylinder. Sinusoidal modulations were machined onto the surface of the foil toward the ablator. X-rays from the hohlraum ablated the CH(Br), launching a series of shocks into the package which compressed it and accelerated it away from the hohlraum wall. Conical shields between the central portion of the hohlraum and the ends protected the package from a direct view of the spots where the laser beams struck the hohlraum wall. The shields were intended to prevent preheat of the package by more energetic x-rays generated in the laser spot, particularly the 2.5-4 keV Au M band. The two remaining Nova beams were directed at a Sc foil to generate a large area (0.7 mm diameter) 4.3 keV backlighter. A pinhole camera imaged the backlit foil onto a gated microchannel plate⁹ to give face-on radiographic images of the accelerated foil. The growth of modulations at the CH(Br)-metal interface may be inferred from variations in the optical depth of the package.

We used shaped laser pulses to generate multiple shocks to accelerate the metal foils without melting them. To reach pressures above the melt pressure on the principal hughoniot, it was necessary to use at least two shocks, which were timed to break out sequentially from the back of the package. A third shock was generated when the rarefaction from release of the back surface returned and was reflected from the ablation front. It is difficult to obtain shockless acceleration on Nova because practical pulse lengths are comparable to the sound transit time through the foil.

Kalantar et al.³ show results from the first set of Nova experiments, which used Cu foils driven at a peak pressure of 3 Mbar. The preliminary analysis shown at the Marseilles meeting suggested that greater strength than that predicted by the Steinberg model was needed to fit the experimental data. Modeling which takes into account the foil thicknesses and laser energies of the individual shots fits the data whether purely fluid behavior or nominal Steinberg strength is assumed. The effect of nominal strength is too small to be resolved for our experimental uncertainties. Measured growth factors at 20 μm wavelength, 1 μm amplitude, and 50 μm wavelength, 2.5 μm amplitude, together with simulations with and without strength, are shown in Figure 2.

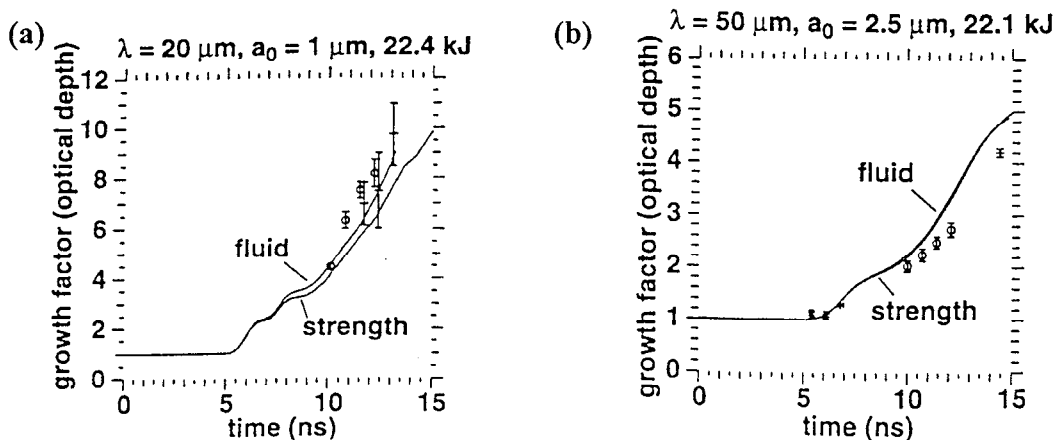


Figure 2. (a) Measured modulation growth factor vs. time for Cu foils, 20 μm wavelength, and simulations without (fluid) and with strength; (b) same for 50 μm wavelength. Results shown are for 2 or 3 shots with similar laser energies, compared with simulations with drives appropriate for those energies. The full Cu data set includes several more shots with different energies, for which the simulation fits are comparable to these cases.

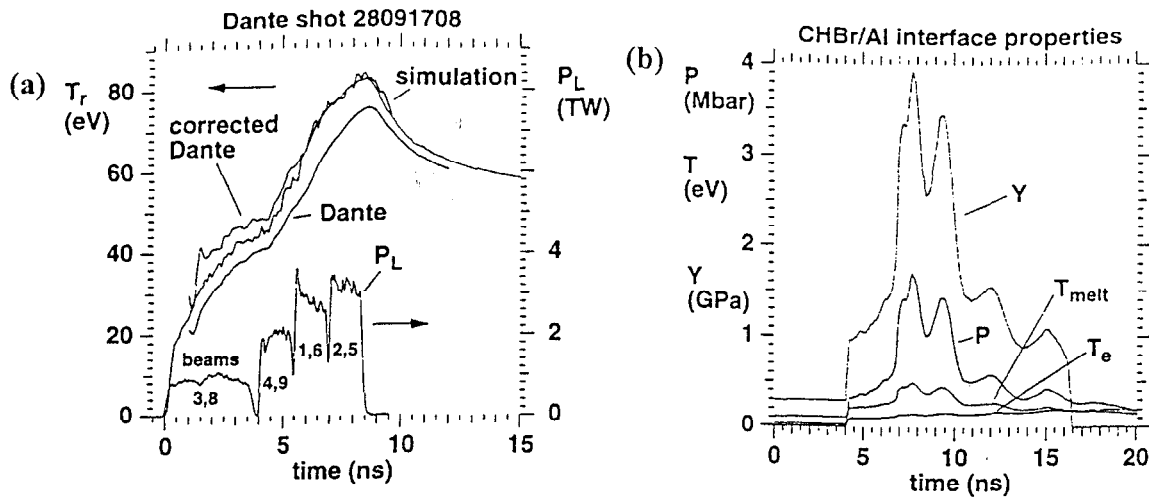


Figure 3. (a) Drive for Al experiment. Laser power vs. time uses scale on right; each segment of the pulse uses one pair of beams. X-ray drive uses left scale. Dante measured radiation temperature, albedo-corrected Dante, and drive simulated with LASNEX are shown. (b) Pressure, material temperature (T_e), yield strength (Y) and melt temperature vs. time at the ablator-Al interface, from a 1-D simulation.

Consequently, the experiment was redesigned to use Al, for which larger strength effects are predicted than for Cu. The drive was also redesigned. Figure 3a shows the laser power and resulting x-ray drive for the Al design (which may be compared with Figure 2 in Kalantar *et al.*) The foot of the pulse is higher and longer than for the Cu design in order to assure that the second shock does not overtake the first before it breaks out of the foil. The peak power part of the pulse has been lengthened in order to give a longer interval of acceleration. Because of Nova energy constraints, the peak power is lower than for the Cu design. We used $0.35 \mu\text{m}$ light for this experiment vs. $0.53 \mu\text{m}$ for the Cu experiment as the former is measured on Nova with greater precision. The new design also uses staggered laser beams; that is, a different pair of beams is used to produce each segment of the pulse shape. This gives higher conversion efficiency of the laser light to the third harmonic than use of a single shaped pulse for all beams.

The new design gives a first shock pressure of 300 kbar and a peak pressure of 1.7 Mbar in the Al. The simulated pressure, temperature, and yield strength vs. time at the ablator-Al interface are shown in Fig. 3b. The melt temperature is from a modified Lindemann law, $T_m = T_{m0} e^{2a(1-\eta)} \eta^{2(\gamma_0 - a - 1/3)}$. Here, T_{m0} is the melt temperature at constant volume, $\eta = \rho/\rho_0$ is the compression, γ_0 is the Grüneisen gamma, and a is the coefficient of volume dependence of γ . The strain rate is up to $2 \times 10^8 \text{ s}^{-1}$, which is very large compared to laboratory or explosive-drive experiments. The yield strength of Al at 1.7 Mbar reaches nearly 4 GPa due to the increase with pressure, and is about the same as that of Cu at 3 Mbar because Al has a stronger pressure dependence than Cu in the Steinberg model. However, the lower density of Al raises the critical amplitude for stability in the Nizovtsev and Rayevsky formula. A comparison of the critical amplitudes is shown in Fig. 4. The experimental amplitudes in the figure are values after compression. We were also able to employ lower initial amplitudes for Al than for Cu since the less massive Al foils moved further, giving larger growth. All of the Al experiments had $0.5 \mu\text{m}$ initial amplitude. Finally, by using $5 \mu\text{m}$ diameter pinholes we were able to measure growth of $10 \mu\text{m}$ wavelengths. It can be seen that the Al design permits experiments straddling the stability threshold while the Cu experiments are substantially

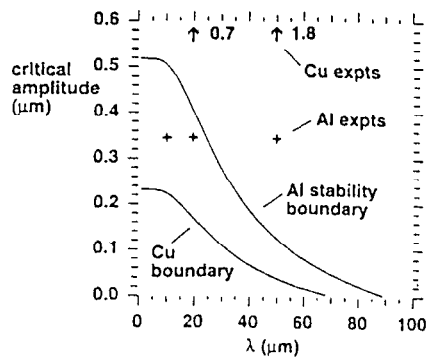


Figure 4. Stability boundary from Nizovtsev and Rayevsky based on simulated time-average conditions for Nova Cu and Al experiments. Amplitudes less than the critical amplitude are predicted to be stable. Experimental wavelengths and post-shock amplitudes are shown with symbols.

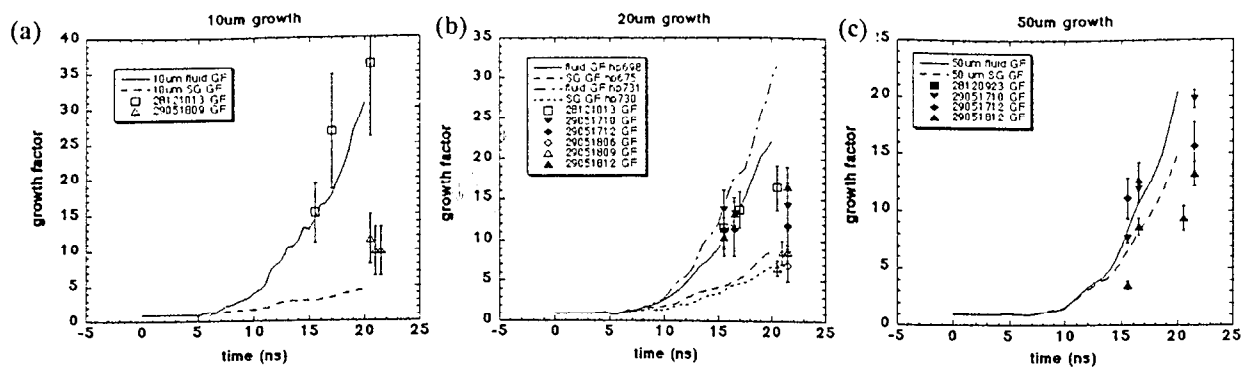


Figure 5. Modulation growth factor vs. time for the Al experiment, wavelengths of 10 μm , 20 μm , 50 μm . Lines are simulations with or without strength. Simulations for the drives of two different shots are shown for the 20 μm case. Symbols are data; open symbols for targets with 10 μm and 20 μm side-by-side, filled symbols for targets with 20 μm and 50 μm side-by-side.

above the threshold. Note that the points in the figure use parameters which were time averaged over the main interval of acceleration, 8-12 ns for the Al design and 6-9 ns for Cu. Most parameters vary substantially even over this limited time interval. Also, this stability threshold is based upon elastic response. As pointed out by Legrande¹⁰, even unmodulated foils are mostly plastic during acceleration for this experiment, due to the unsteady acceleration. Legrande points out that plastic flow is equivalent to viscous flow (also noted by Colvin¹¹). Viscosity is also more effective at reducing the growth of short wavelengths but the reduction is not dependent upon amplitude and does not give absolute stability at finite wavelength.

X-ray drive was measured directly with the Dante¹² x-ray diode diagnostic, which observes emission of a patch of the hohlraum wall through a diagnostic hole. The Dante measurement was corrected for the wall albedo to get the x-ray flux incident upon the wall, which is equivalent to the flux onto a package. At radiation temperatures of 30-80 eV, the albedo correction is larger and more uncertain than that for $T_r \sim 150\text{-}250$ eV more commonly employed for ICF. The x-ray drive was also predicted by integrated hohlraum simulations. These assumed 2-D axial symmetry, which may be less accurate for the staggered beam drive than for cases in which 8-10 beams are on at the same time. Figure 3a includes the measured and albedo-corrected Dante drives, as well as the drive simulated by LASNEX. Finally, the motion of the foil was measured by streaked side-on imaging. All of these techniques are consistent within experimental uncertainties.

3. Simulations

Foil acceleration and instability growth were simulated with LASNEX. Calculations were run in a Lagrangian mode. The strength modeling assumed elastic-perfectly plastic flow using the Steinberg constitutive model, which is not rate dependent for Cu or Al. The Steinberg model gives for the form of the shear modulus, $\mu = \mu_0 [1 + AP\eta^{-1/3} - B(T - T_0)]$, where P and T are the pressure and temperature, μ_0 is the initial shear modulus, and A and B are fitting coefficients. For Al, $A = 6.52 \text{ Mbar}^{-1}$, giving substantial increase in strength with pressure. The yield strength is $Y = Y_0(1 + \beta\epsilon)^n \mu / \mu_0$, where μ_0 is the yield strength at the Hugoniot elastic limit, ϵ is the equivalent plastic strain, and β and n are fitting parameters for work hardening. Note that Y increases with pressure in the same manner as μ . If the experiments become good enough to test the constitutive model, other models may readily be inserted into the calculational method. The equation of state is the Thomas-Fermi QEOS¹³ model. Simulations were postprocessed for comparison to radiography data. Transmission of backlighter photons was calculated using rays propagated through the mesh. These calculations assumed a monochromatic backlighter. Calculated profiles of optical depth vs. transverse position were corrected for the measured modulation transfer function (mtf) of the gated imager. The result is profiles of optical depth as resolved by the instrument, which should be directly comparable to data lineouts. Modulation growth factors were obtained by dividing the contrast by the initial contrast to get optical depth growth factor vs. time. Perturbations are sufficiently linear that this growth factor is not very different from the growth factor in modulation of Al column density, $\rho\Delta x$. Consequently, the simulated growth factors are fairly insensitive to backlighter spectrum and instrument resolution.

Figure 5 shows simulated modulation growth factors for wavelengths of 10, 20, and 50 μm from calculations employing the Steinberg strength model, and also for simulations assuming no strength. The growth factors are in optical depth as would be resolved by the instrument, as described above. The effect of strength is modest for the 50 μm wavelength, while growth for 20 μm is reduced by a factor of more than two, and the 10 μm case is predicted to

have little growth for the case with strength. These results are in qualitative agreement with the predictions of the Nizovtsev and Rayevsky theory as the 10 μm case is well below the stability boundary, the 50 μm case is well above it, and the 20 μm case is near the boundary.

4. Al instability growth measurements

Measured modulation growth factors are also shown in Figure 5. Data from experiments with 10 μm and 20 μm modulations side-by-side are shown as open symbols while results from target combining 20 μm and 50 μm modulations are plotted as filled symbols. The data shows a range of growth from near predictions for the fluid case to substantially below fluid, near the simulations assuming strength. There is some shot-to-shot variation in the fabricated foil thicknesses and in the laser power histories, which were measured for every shot. Drives for individual shots have been approximated by scaling from the drive measurement according to laser power history. Fig. 5b shows the predicted growth factor difference for two representative shots with differing thicknesses and laser powers. The variation from this source is not large enough to account for the range in measured growth for 10 and 20 μm wavelength.

We have considered several possible causes for the shot-to-shot variation in measured growth. Pinhole degradation may have affected some shots. The instrument response has been checked by observing contrast for undriven foils with large machined modulation. After one such measurement showed lower than expected contrast, apparently due to debris in the pinholes, the pinholes were replaced. All of the data shown in Fig. 5 are from measurements made with new pinholes, for which the instrumental resolution was measured to be satisfactory. Additional data from a larger number of shots for which the pinhole status is uncertain span approximately the same range in growth factor.

Also, there is variation in grain structure between different foils. All of the foils with the 10 + 20 μm wavelength combination were cut from one piece of aluminum, and the 20 + 50 μm combination from another piece. Figure 6a shows a micrograph of an unmodulated section of one of the aluminum samples, with grain structure apparent. Similar-looking structure is seen in the experimental radiograph, Figure 6b. The structure in the radiograph is unlikely to have grown up from random surface finish modulation as the deviations from the intended sinusoid were measured to be much smaller in amplitude than the sinusoid, ~ 5 nm. The grain structure is elongated in the direction in which the aluminum plate was rolled during the course of its preparation. Comparison of perturbation growth between foils with modulation machined parallel or perpendicular to the rolling direction shows no apparent correlation with rolling direction.

Preheat is another factor which could affect modulation growth. Preheat of only 0.1-0.2 eV, would cause all or part of the aluminum to melt after shock compression. One known preheat source in laser hohlraums is x-rays from the Au M band in the 2.5-4 keV band, emitted by plasma directly heated by the laser. Shielded hohlraums were used for this experiment to block lines of sight to the foil from the laser spots on the hohlraum wall. However, during the laser pulse the hohlraum fills with plasma, and the package is not shielded from much of the laser path between the entrance hole and the wall. Hohlraum simulations predict that flux in the 2.5-4 keV band is only about 0.05% of the total x-ray flux striking the package location, while foil simulations indicate that an M band flux fraction of $\sim 0.5\%$ would eliminate most of the stabilizing effect of strength. The predicted M band fraction of 0.05% has negligible

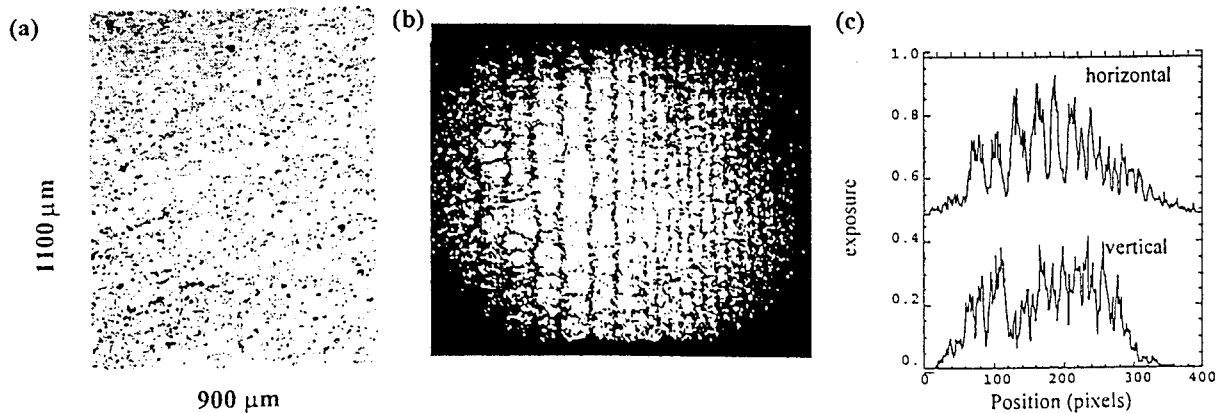


Figure 6. (a) micrograph of one of the Al samples from which experimental foils were cut; (b) radiograph at a time of 21.6 ns showing 50 μm and 20 μm modulations and 3-D structure; (c) horizontal and vertical lineouts from (b) showing that amplitudes of 2-D and 3-D structure are comparable.

effect upon the predicted strength stabilization. For comparison, typical ICF hohlraums without shielding and driven to higher radiation temperatures of 150-250 eV commonly have M band fractions of 2-10%.

However, the 2-D hohlraum simulation fails to represent important 3-D effects, most notably the effect of individual beams turning on and off during the staggered beam pulse. When a new beam turns on, it goes into a part of the hohlraum which did not have a beam going through it earlier in the pulse. Beams create lower density channels by heating the plasma through which they pass. When a new beam is turned on, it hits denser plasma ablated by x-rays from wall not illuminated by the laser. We made a crude attempt to estimate this effect with a 2-D simulation. A hohlraum was heated with a uniform thermal x-ray source until the middle of the pulse, to give a plasma configuration corresponding to x-ray heated walls. Then a laser beam was turned on to see the effect of introducing a beam into cooler plasma. This simulation predicted an M band flux onto the sample of 0.3-0.5%. Shot to shot preheat variation could be caused by beam pointing variations. If the preheat is near the melt threshold, growth factors could be sensitive to small variations.

The entire foil thickness is not melted during most of its acceleration by an M band fraction of 0.5%. Since the melt temperature is increased several-fold by compression, and the pressure goes to zero at the free surface of the foil, increasing preheat melts the foil progressively from the free surface toward the ablator interface. Similarly, dropping drive late in the x-ray pulse results in the foil melting from decompression.

5. Preheat measurement

Since preheat is a critical issue for this experiment, it would be very valuable to measure foil preheating directly. Unfortunately, this is quite difficult to do. Three techniques which could potentially give information about preheat are drive spectrum measurement, optical interferometry, and dynamic x-ray diffraction.

It seems unlikely that we could measure an M band fraction in the drive flux to tenths of a percent of the total flux. Current measurements are sensitive to ~1% of the total flux. Furthermore, it is not certain where in the hohlraum preheat radiation might be coming from. The sample sees a hemisphere of illumination while the Dante looks along a single angle. The normal Dante line of sight views x-ray heated hohlraum wall, which is not expected to emit M band radiation. The instrument is not in a position to look along the line of sight from the package into the primary (laser-heated) section of the hohlraum.

We have attempted to measure preheat by measuring motion of foil surfaces with an optical interferometer¹⁴. This instrument was originally configured as a Michelson interferometer, which measure fringes between a beam reflected off of the target and a reference beam. We used this instrument to measure the time of shock breakout from a 17 μm -thick Al foil with no CH(Br) ablator, driven by the pulse of the earlier Cu RT experiment. Our goal for that measurement was to diagnose the drive of the foot of the pulse. We used an Al foil because we did not get a good enough reflection off Cu to get fringes. Figure 7a shows the data, recorded with a streak camera, showing fringe motion. Figure 7b shows foil surface motion inferred from fringe motion and simulation fits. A small amount of motion is seen before breakout of the shock. This can be fit by assuming 200 K of preheat before 3.5 ns, which causes ~0.15 μm of surface motion just from thermal expansion. The preheat was added as *ad hoc* volumetric energy deposition. This amount of preheat would not have a significant effect upon the RT experiment. However, this experiment is sensitive to preheat occurring before the shock breakout time of 4 ns, while M band preheat is likely to be higher later in time, during peak drive.

For our recent experiments, the instrument was configured as a VISAR (Velocity Interferometer System for Any Reflector). Both beams were reflected off of the experimental package, one delayed in time with respect to the other. The fringe shift is determined by velocity if the time separation is small. However, we used the VISAR as a position interferometer by timing the beams so that the earlier one was reflected before the drive started. The package employed for a preheat diagnostic consisted of 19 μm of CH(Br), 42 μm of CH, and 3 μm of Al. The undoped CH was inserted between the ablator and the Al to delay the arrival of the shock at the back surface until after most of the drive, at ~10 ns. Thin aluminum foil was used because the mean free path of M band radiation in Al is ~3 μm , so M band preheat would not cause a visible effect at the rear surface of a 20 μm thick Al foil as used for the RT measurements. Figure 7c shows motion of the surface of this package from a single successful shot with rather poor fringe quality. The data are consistent with simulations assuming M band preheat of ~0.5% of the x-ray flux. Confidence in this result is limited both by the data quality and by the fact that interpretation is based upon the simulation fit, which is subject to modeling uncertainties.

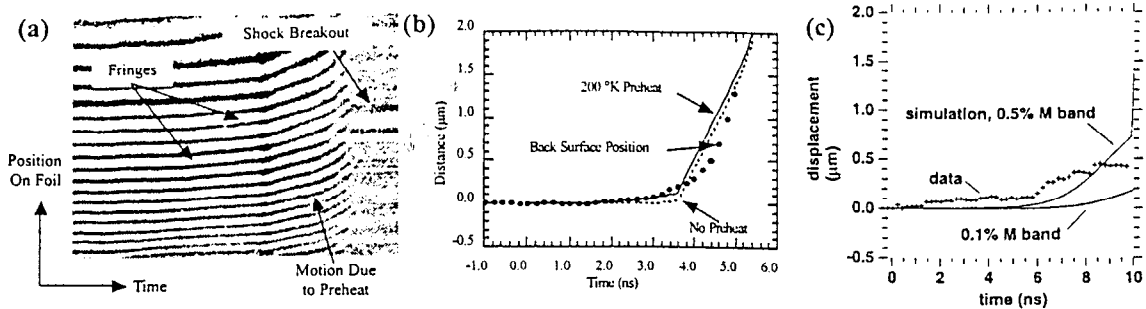


Figure 7. (a) Streaked image of Michelson interferometer data for a 17 μm -thick Al foil with no CH(Br) ablator and the drive of the Cu RT experiment. (b) Back surface position vs. time inferred from the fringe motion of (a) and simulations with and without *ad hoc* preheat of 200 K. (c) Interferometric measurement of motion vs. time for a 3 μm Al foil, covered with 42 μm CH and 19 μm CH(Br) ablator. Simulation results are shown for drives with 0.1% and 0.5% of the total x-ray flux in the spectral range of the Au M band.

Dynamic x-ray diffraction is the most promising diagnostic of the solid state of the metal foils. We have performed dynamic Bragg diffraction by reflecting a point source of x-rays off of the rear surface of a single crystal sample. Shock compression changes the Bragg angle, giving a shift in position of the diffracted signal, which is recorded with a streak camera. The measurement gives compression vs. time, as well as confirming the continued existence of a crystal lattice. Data showing diffraction from shock-compressed material was obtained on Nova for Si crystals driven with flat top pulses¹⁵. However, in a number of attempts we were not able to see shifted diffraction features indicating compression from Cu or Al crystals. Problems with the quality of the single crystal foils probably played a role. We have seen diffraction signals indicating compression of Cu from more recent experiments on the Trident and Omega lasers using direct drive with flat top pulses. Work is continuing on this project, which we hope may eventually be able to confirm the solid state of foils driven to megabar pressures with shaped pulses.

6. Conclusions

RT growth of preimposed modulations of wavelength 10, 20, and 50 μm has been measured in Al foils accelerated by pressures of up to 1.5 Mbar. Observed growth varies between nominally identical shots, with some shots showing growth near simulation predictions which assume no strength, while others show significantly lower growth, in some cases near predictions of simulations including strength. One plausible hypothesis for the variable growth is variable x-ray preheat from Au M band radiation. Partial melting and substantial reduction of the hydrodynamic effect of strength is predicted for M band flux of $\sim 0.5\%$ of the total flux. Hohraum simulations offer some support for the plausibility of preheat of this order. Measurements of foil surface motion by optical interferometry also show evidence of preheat. Dynamic x-ray diffraction is being developed as a direct measure of the material state. More development of these diagnostics is needed.

Scaling of this design to NIF energies indicates that pressures up to 10 Mbar may be reached. However, it will be necessary to have diagnostics of preheat and melting in order to verify the sample conditions that are achieved. Iteration of the design, guided by such measurements, may be needed. Ongoing experiments on the Omega laser are directed at development of dynamic diffraction and preheat diagnostics.

This work was performed under the auspices of the U. S. Department of Energy by the Lawrence Livermore National Laboratory under Contract W-7405-ENG-48.

References

- ¹ J. F. Barnes, P.J. Blewett, R. G. McQueen, K.A. Meyers, and D. Venable, *J. Appl. Phys.* **45**, 727 (1974).
- ² A. I. Lebedev, P. N. Nizovtsev, V. A. Rayevsky, in the Proceedings of the 4th International Workshop on the Physics of Compressible Turbulent Mixing, 29 March - 1 April, Cambridge, England (Cambridge University Press, 1993), p. 81; A. I. Lebedev, P.N. Nizovtsev, V.A. Rayevsky, and V.P. Soloviov, in *The Physics of Compressible Turbulent Mixing*, G. Jourdan and L. Houas eds., p. 307, (1997).
- ³ D. H. Kalantar, B.A. Remington, E.A. Chandler, J.D. Colvin, D.L. Griswold, R.E. Turner, S.V. Weber, and L.G. Wiley, in *The Physics of Compressible Turbulent Mixing*, G. Jourdan and L. Houas eds., p. 232, (1997).
- ⁴ H. J. Melosh, *Impact Cratering: A Geologic Process* (Oxford U. Press, New York, 1989); O'keefe and T. J. Ahrens, *J. Geo. Res.* **98**, 17011 (1993).
- ⁵ R. Jeanloz and B. Ramanowicz, *Physics Today* **50**, 22 (1997).

- ⁶ D.G. Brasher, D. J. Butler, *Advanced Materials & Processes*, **147**, 37 (1995).
- ⁷ P. N. Nizovtsev and V. A. Rayevsky, *VANT. Ser. Teor. I Prikl. Fizika* **3**, 11 (1991).
- ⁸ D. J. Steinberg, S. G. Cochran, M. W. Guinan, *J. Appl. Phys.* **51**, 1498-1504 (1980).
- ⁹ K. S. Budil, *et al*, *Rev. Sci. Instrum.* **67**, 485-488 (1996).
- ¹⁰ M. Legrande, *Seventh International Workshop of the Physics of Compressible Turbulent Mixing*.
- ¹¹ J. D. Colvin, L. G. Wiley, E. A. Chandler, B. A. Remington, and D. H. Kalantar, in *The Physics of Compressible Turbulent Mixing*, G. Jourdan and L. Houas eds., p. 134, (1997).
- ¹² H. N. Kornblum, R. L. Kauffman, J. A. Smith, *Rev. Sci. Instrum.* **57**, 2179-2181 (1986).
- ¹³ R. M. More, K. H. Warren, D. A. Young, and G. B. Zimmerman, *Phys. Fluids* **31**, 3059 (1988).
- ¹⁴ D. M. Gold, P.M. Celliers, G.W. Collins, L.B. DaSilva, R.C. Cauble, D.H. Kalantar, S.V. Weber, and B.A. Remington, "Optical interferometry diagnostics in laser-driven equation of state experiments", to be published in *Shock Compression in Condensed Matter-1999*, edited by M.D. Furnish, AIP Conference Proceedings, New York 1999.
- ¹⁵ D. H. Kalantar, E. A. Chandler, J. D. Colvin, R. Lee, B. A. Remington, S. V. Weber, A. Hauer, J. S. Wark, A. Loveridge, B. H. Failor, M. A. Meyers, and G. Ravichandran, *Rev. Sci. Instrum.* **70**, 629 (1999).